Journal of Computational Physics 227 (2008) 10094–10107

Contents lists available at ScienceDirect

Journal of Computational Physics

journal homepage: www.elsevier.com/locate/jcp

# Collision of multi-particle and general shape objects in a viscous fluid

A.M. Ardekani, S. Dabiri, R.H. Rangel *

*Department of Mechanical and Aerospace Engineering, University of California, Irvine, CA 92697-3975, United States*

ARTICLE INFO

*Article history:*
Received 15 January 2008
Received in revised form 9 July 2008
Accepted 14 August 2008
Available online 3 September 2008

*Keywords:*
Collision
Particulate flow
Numerical simulation
Finite-volume method

ABSTRACT

The dynamics of particle–particle collisions in a viscous fluid are numerically investigated. A distributed-Lagrange-multiplier-based computational method in a solid-fluid system is developed and a collision strategy for general shape objects is presented. In earlier methods, a repulsive force is applied to the particles when their separation is less than a critical value and, depending on the magnitude of this repulsive force, collision may not be prevented or particles may bounce unrealistically. In the present method, upon collision of two or more particles, a uniformly distributed force is added to each particle. The contact force is calculated and the relative velocity of the particles along their line of center vanishes. For non-spherical (or non-cylindrical in 2-D) particles the force due to collision may lead to a torque around the center of mass of each particle. In this situation, the uniform distributed force is modified in order to create a net torque around the center of mass of each particle without changing the net force applied to that particle. The contact force is impulsive at the onset of the collision process and decreases smoothly to zero when contact ends. Particles separate from each other when the contact force vanishes and subsequently, a rigidity constraint is satisfied for each particle separately. Results for systems of multi-particle and general shape objects in a viscous fluid are presented.



## 1. Introduction

In order to accurately predict the behavior of particulate flows, a fundamental knowledge of the mechanisms of particle collision is required. Classical lubrication theory predicts that the lubrication force becomes singular as the distance between two smooth spheres approaches zero and hence prevents smooth spheres from touching. In practice, no general numerical method can afford the computational cost of resolving the flow in the narrow gaps between closely-spaced particles and some modelling is needed. In reality, the surface of particles has some roughness and the bumps make physical contact due to the discrete molecular nature of the fluid and/or attractive London-van der Waals forces. Thus, further approach is prevented, and solid–solid contact occurs [1].

Davis [2] considered a roll/slip model and a stick/rotate model for the motion of touching spheres in Stokes flow and found that the roll/slip model is consistent with experiments [3]. Ekiel-Jezewska et al. [4,5] used the roll/slip model of contact for interaction between two spherical particles immersed in a viscous fluid. Comparison of the model with experimental results for the settling motion of a sphere in the vicinity of another fixed sphere showed good agreement. Zhang et al. [6] considered collision of a sphere onto a stationary sphere at finite Reynolds numbers. Their experimental results are in agreement with the mechanistic model they developed and the numerical results using the lattice Boltzmann method. Lin et al. [7] studied an elastic collision between two cylindrical particles also using the lattice Boltzmann method.

Particulate flow simulations under the Stokes-flow assumption have been conducted using Stokesian-dynamics techniques [8]. For dilute suspensions, the unsteady motion of two solid spheres has also been analyzed [9]. However, for intermediate Rey-

* Corresponding author.
*E-mail address:* rhrangel@uci.edu (R.H. Rangel).

0021-9991/$ - see front matter © 2008 Elsevier Inc. All rights reserved.
doi:10.1016/j.jcp.2008.08.014

nolds numbers the use of numerical simulation is generally unavoidable. A distributed Lagrange multiplier (DLM)-based computational method is used here in order to simulate particulate flow and collisions between particles. Glowinski et al. [10,11] employed a finite-element approach utilizing DLM with a fixed structured grid thus eliminating the need of remeshing required for unstructured boundary-fitted grids. In DLM, the entire domain is treated as a fluid but the fluid inside the particle domain satisfies a rigidity constraint by using Lagrange multipliers. The DLM solution can be formulated by forcing the deformation tensor in the particle domain to be zero thus eliminating $\mathbf{U}$ and $\boldsymbol{\omega}$ as variables from the coupled system of equations, where $\mathbf{U}$ and $\boldsymbol{\omega}$ are the translational and angular velocity of the particle, respectively [12,13]. This formulation introduces a stress field in the particle domain similar to the pressure in an incompressible fluid. Sharma et al. [14] presented a formulation based on DLM for steady Stokes flow using a control-volume method. The numerical simulation used in the present paper is based on the DLM method implemented using a control-volume approach and the SIMPLE [15] algorithm.

Previous analyses show that smooth particles do not come into physical contact under finite forces [1]. However, as explained earlier in physical situations, particle surface has some roughness and solid–solid contact occurs due to the discrete molecular nature of the fluid and/or attractive London-van der Waals forces. In numerical simulations, contact can occur due to numerical truncation errors and thus it is necessary to use a reliable collision strategy. In earlier approaches, a repulsive force was applied to the particles when their separation was less than a critical value. In order to have at most one rigid body motion constraint at each node, the particles were limited to be more than one grid element apart as described by Glowinski et al. [11] and Singh et al. [16]. Singh et al. [17] modified DLM in order to eliminate the so-called security zone by allowing the particles to be close to each other and even overlap. They used the constraint of the closer particle to the node, in order to prevent the conflict of having two rigid-body constraints at one node. The repulsive force is applied when the particles overlap. In these collision schemes, the choice of the stiffness parameter is important. If the stiffness parameter is too small, the collision will not be prevented and if it is too large, the repulsive force will be too strong and particles will bounce unrealistically as explained by Hu et al. [18]. Another approach is to use the solid-body collision model which neglects the fluid during the collision process. In this method, a fully explicit scheme is used for updating particle positions and velocities but the method can be unstable as noted by Hu et al. [18]. Ardekani and Rangel [19] developed a collision strategy, in which no repulsive force is applied to the particles and instead the contact force between particles is computed. By using conservation of linear momentum along the particles line of centers, both particles can be rigidified together. One advantage of this method is that the particle velocity is not updated explicitly thus preventing numerical instabilities. Furthermore, the particles do not overlap and we do not have two rigid body motion constraints (one for each particle) at one node. Contact starts when the distance between particles becomes zero for smooth particles and ends when the contact force becomes zero since the particles cannot apply a tensile force to each other. For particles with surface roughness, the contact starts when their separation reaches the roughness height. Since the normal force applied to particles is calculated, one could use this strategy for collisions including friction. Here, we generalize the numerical investigation of the collision process by Ardekani and Rangel [19] for multi-particle and general shape objects.

## 2. Theoretical development

The governing equations in the fluid domain for a particulate flow are

$$\rho_{\mathrm{f}} \frac{\mathrm{D}\mathbf{u}}{\mathrm{D}t} = \nabla \cdot \boldsymbol{\sigma} + \rho_{\mathrm{f}}\mathbf{g} \quad \text{in } \Omega \setminus \overline{P} \tag{1}$$

$$\nabla \cdot \mathbf{u} = 0 \quad \text{in } \Omega \setminus \overline{P} \tag{2}$$

$$\mathbf{u} = \mathbf{U}_{\mathrm{p}_i} + \boldsymbol{\omega}_i \times \mathbf{r} \quad \text{on } \partial P \tag{3}$$

$$\mathbf{u}|_{t=0} = \mathbf{u}_0(\mathbf{x}) \quad \text{in } \Omega \setminus \overline{P} \tag{4}$$

in addition to the outer boundary conditions on $\Gamma$. In these equations, $\Gamma$ represents the fluid boundary which is not shared with the particle. The solid domain and its boundary are denoted by $P$ and $\partial P$, respectively. The computational domain is $\Omega$, including both the fluid and the particle, $\mathbf{u}$ is the fluid velocity, $\mathbf{g}$ is the acceleration of gravity, $\rho_{\mathrm{f}}$ is the fluid density, $\mathbf{n}$ is the normal unit vector on the surface, $\mathbf{U}_{\mathrm{p}_i}$ is the $i$th particle velocity, and $\omega_i$ is the $i$th particle angular velocity. The initial velocity $\mathbf{u}_0$ satisfies the continuity equation, $\boldsymbol{\sigma} = -p\mathbf{I} + \boldsymbol{\tau}$ is the stress tensor, $p$ is the pressure field, $\mathbf{I}$ is the identity tensor, and $\boldsymbol{\tau}$ is the viscous stress:

$$\boldsymbol{\tau} = 2\mu\mathbf{D}[\mathbf{u}] = \mu[\nabla\mathbf{u} + (\nabla\mathbf{u})^{\mathrm{T}}] \tag{5}$$

The governing equations in the particle domain are

$$\rho_{\mathrm{P}} \frac{\mathrm{D}\mathbf{u}}{\mathrm{D}t} = \nabla \cdot \boldsymbol{\sigma} + \rho_{\mathrm{P}}\mathbf{g} \quad \text{in } P \tag{6}$$

$$\nabla \cdot \mathbf{u} = 0 \quad \text{in } P \tag{7}$$

$$\mathbf{D}[\mathbf{u}] = 0 \quad \text{in } P \tag{8}$$

$$\mathbf{u} = \mathbf{U}_{\mathrm{p}_i} + \boldsymbol{\omega}_i \times \mathbf{r} \quad \text{on } \partial P \tag{9}$$

$$\mathbf{u}|_{t=0} = \mathbf{u}_0(\mathbf{x}) \quad \text{in } P \tag{10}$$

where $\rho_P$ is the particle density. Eq. (8) satisfies the continuity equation but in order to facilitate numerical implementation, Eq. (7) is retained. As pointed out by Sharma et al. [14], the rigidity constraint gives rise to a stress field inside the particle which is a function of three scalar Lagrange multipliers for three dimensional problems. Thus

$$\boldsymbol{\sigma} = -p\mathbf{I} + \boldsymbol{\tau} + \mathbf{D}[\boldsymbol{\lambda}] \tag{11}$$

where $\boldsymbol{\lambda}$ represents the Lagrange multipliers and $\boldsymbol{\tau}$ is zero inside the particle due to the rigidity constraint. The governing equations in the entire domain can be combined as

$$\rho\frac{D\mathbf{u}}{Dt} = \nabla\cdot\boldsymbol{\sigma} + \rho\mathbf{g} + \mathbf{f} \quad \text{in } \Omega \tag{12}$$

$$\nabla\cdot\mathbf{u} = 0 \quad \text{in } \Omega \tag{13}$$

$$\mathbf{u}|_{t=0} = \mathbf{u}_0(\mathbf{x}) \quad \text{in } \Omega \tag{14}$$

where

$$\rho = \begin{cases} \rho_f & \text{in } \Omega\setminus\overline{P} \\ \rho_P & \text{in } P \end{cases} \tag{15}$$

in addition to the outer boundary conditions on $\Gamma$. In the above equations, $\mathbf{f} = \nabla\cdot\mathbf{D}[\boldsymbol{\lambda}]$ is zero everywhere except in the particle domain and leads to the rigid-body motion inside the particle.

## 3. Numerical implementation

A finite-volume method using a staggered grid for incompressible flow is implemented. The SIMPLE algorithm [15] is used to solve the fluid equations with modifications to account for the presence of particles. The Crank–Nicolson scheme is used for time discretization.

The discretised momentum equations for 2-D flows in the $x$ and $y$ directions are

$$a_{i,J}u_{i,J} = \sum a_{nb}u_{nb} - \frac{p_{I,J} - p_{I-1,J}}{\delta x_u}\Delta V_u + b_{i,J} + F_{xi,J} \tag{16}$$

$$a_{I,j}v_{I,j} = \sum a_{nb}v_{nb} - \frac{p_{I,J} - p_{I,J-1}}{\delta y_v}\Delta V_v + b_{I,j} + F_{yI,j} \tag{17}$$

where $\Delta V_u$ and $\Delta V_v$ are the volumes of the $u$-cell and $v$-cell, respectively; $u$ and $v$ represent the horizontal and vertical components of the velocity field; $I$ and $J$ are the nodes at the center of the main control volumes; while $i$ and $j$ represent the nodes at the center of the control volumes for $u$ and $v$, respectively, as shown in Fig. 1. Subscript $nb$ refers to corresponding neighboring staggered control volumes; $b$ is the momentum source term which includes the gravity term; and $\mathbf{F}$ represents the rigidity force which makes the velocity field inside the particle domain satisfy the rigidity constraint.

Following the SIMPLE algorithm and taking the particles into account, the force $\mathbf{F}$ is added as an unknown variable and $\mathbf{F} = \mathbf{F}^* + \mathbf{F}'$ where $\mathbf{F}^*$ is the force predicted at each iteration (the force calculated in the previous iteration) and $\mathbf{F}'$ is the correction force. At each iteration, the rigidity force is defined as

$$F_{xi,J} = F^*_{xi,J} + C\rho_P A_{i,J}(u_{i,J} - u_{Ri,J}) \tag{18}$$

and similarly in the $y$ direction

$$F_{yI,j} = F^*_{yI,j} + C\rho_P A_{I,j}(v_{I,j} - v_{RI,j}) \tag{19}$$

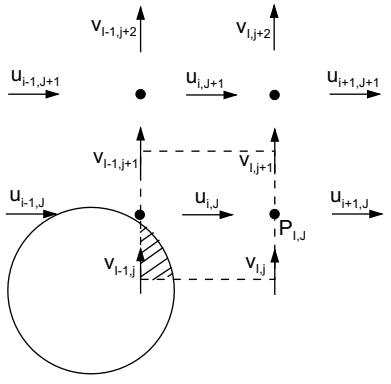


**Fig. 1.** Staggered grid, $u$ control volume and corresponding volume fraction.

where $A_{i,J}$ and $A_{I,j}$ are the areas of the $u$-cell and $v$-cell, respectively; while $\mathbf{u}_R$ is the velocity vector rigidified inside the particle, equal to $\mathbf{u}$ outside the particle domain. $C$ is a dimensional constant defined as $C = -\alpha U_s$, where $\alpha$ is a dimensionless factor whose values are provided in Section 5; $U_s$ is the velocity scale in the problem. In these equations, the force correction is assumed to be proportional to the particle density and grid area since it should be proportional to the grid inertia. This formulation resembles a penalty approach. However, the reason behind Eqs. (18) and (19) is explained as follows. Consider step 1 shown in Fig. 2. If we use the corrected force $F^* + F'$ as a source term to that equation, the velocity field will be the rigidified velocity. Thus

$$a_{i,J} u_{Ri,J} = \sum a_{nb} u_{Rnb} - \frac{p_{I,J} - p_{I-1,J}}{\delta x_u} \Delta V_u + b_{i,J} + F^*_{xi,J} + F'_{xi,J} \tag{20}$$

$$a_{I,j} v_{RI,j} = \sum a_{nb} v_{Rnb} - \frac{p_{I,J} - p_{I,J-1}}{\delta y_v} \Delta V_v + b_{I,j} + F^*_{yI,j} + F'_{yI,j} \tag{21}$$

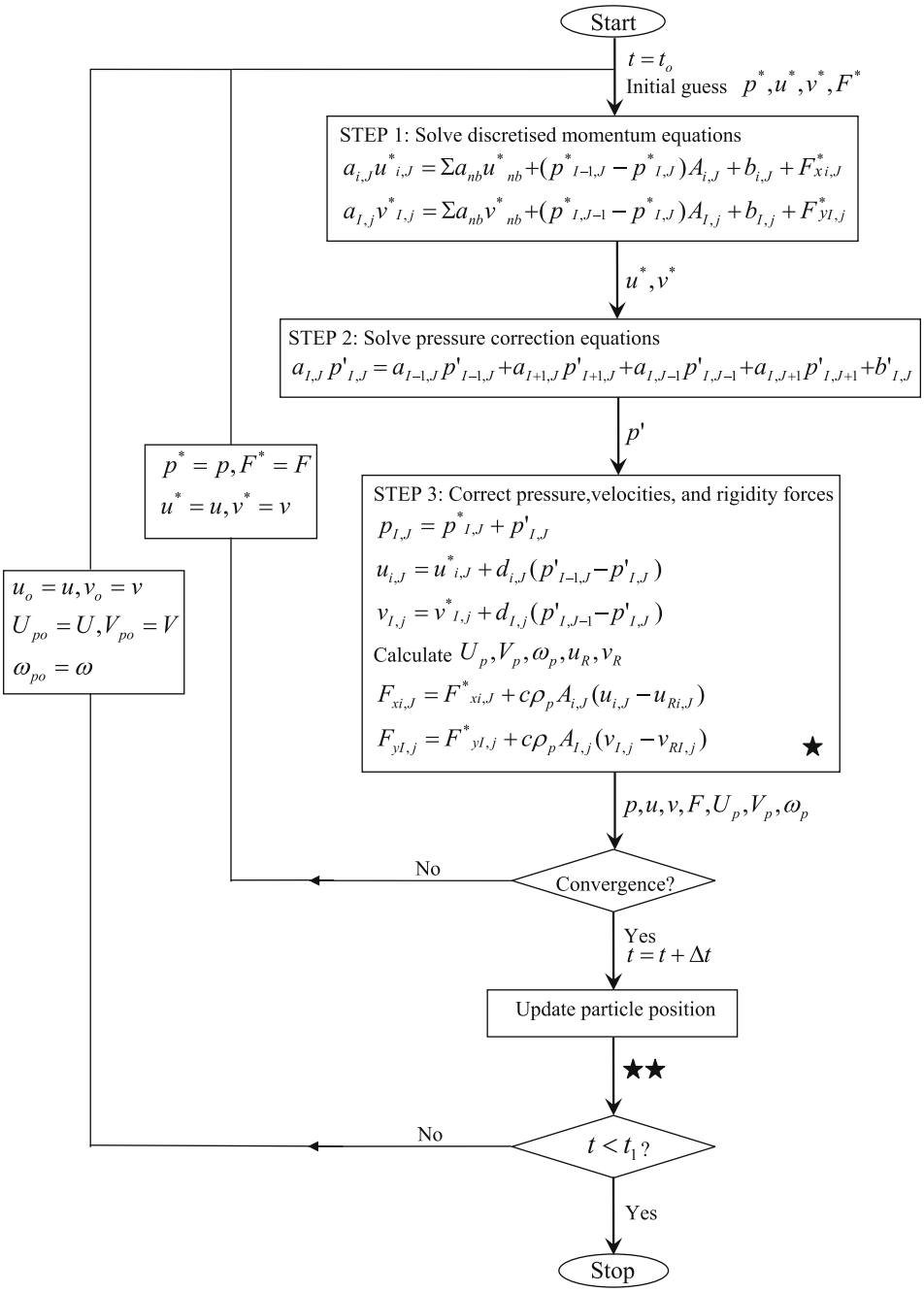


**Fig. 2.** Flowchart.

Subtracting this equation from step 1 shown in Fig. 2, we have

$$a_{i,J}(u_{i,J} - u_{\mathrm{R}i,J}) = \sum a_{nb}(u_{nb} - u_{\mathrm{R}nb}) + F'_{xi,J} \tag{22}$$

$$a_{I,j}(v_{I,j} - v_{\mathrm{R}I,j}) = \sum a_{nb}(v_{nb} - v_{\mathrm{R}nb}) + F'_{yI,j} \tag{23}$$

One can use the following equation to calculate $F'_x$ and $F'_y$ or further simplification can be achieved by neglecting the summation on the right hand side of the above equations. $a_{i,J}$ and $a_{I,j}$ include convection, diffusion, and unsteady terms. The unsteady term is $\rho\frac{\Delta V}{\delta t} = \rho A\frac{\delta x}{\delta t}$, where $\rho$ inside the particle is equal to $\rho_{\mathrm{p}}$ and we let $\frac{\delta x}{\delta t} = U_{\mathrm{s}}$ (the velocity scale) as it is related to the velocity scale through the Courant number. $\mathbf{u}_{\mathrm{R}}$ is defined as follows:

$$\mathbf{u}_{\mathrm{R}} = (1-\phi)\mathbf{u} + \phi\mathbf{u}_{\mathrm{P}} \tag{24}$$

where $\phi$ is the volume fraction occupied by the particle in each control volume, defined separately for $u$ and $v$-cells. For example, as shown in Fig. 1, $\phi_u = \frac{\Delta V_{\mathrm{hatched}}}{\Delta V_u}$. In the present study, $\phi$ is calculated as in [20]. $\mathbf{u}_{\mathrm{P}}$, defined only in the particle domain, can be calculated as follows:

$$\mathbf{u}_{\mathrm{P}} = \mathbf{U}_{\mathrm{P}} + \boldsymbol{\omega}\times\mathbf{r} \tag{25}$$

where $\mathbf{U}_{\mathrm{P}}$ is the particle translational velocity of the center of mass and $\boldsymbol{\omega}$ is the particle angular velocity. By using conservation of linear and angular momentum for the solid particle, one can calculate the particle translational and angular velocities as follows [14] and [20]:

$$M_{\mathrm{P}}\mathbf{U}_{\mathrm{P}} = \int_P \rho\mathbf{u}\,\mathrm{d}\mathbf{x} \quad \text{and} \quad \mathbf{I}_{\mathrm{P}}\boldsymbol{\omega} = \int_P \mathbf{r}\times\rho\mathbf{u}\,\mathrm{d}\mathbf{x} \tag{26}$$

Defining a rigidity force as in Eqs. (18) and (19) guarantees that, upon convergence at each time step, $\mathbf{u} = \mathbf{u}_{\mathrm{R}}$ everywhere in the entire domain. The summation of $F$ over each particle is equal to the external forces applied to that particle, excluding the gravitational and hydrodynamic forces since these two forces are included in Eq. (6). Thus when freely moving particles are not in contact we have

$$\sum_i\sum_J F_{xi,J} = \sum_I\sum_j F_{yI,j} = 0 \tag{27}$$

Using Eqs. (18) and (19) guarantees that the total rigidity force applied to each particle is zero at each iteration. Finally, the modifications due to the presence of the particle can be included by adding $\mathbf{F}$ as a source term in the momentum equations. Eqs. (18) and (19) are solved after the pressure correction step. Fig. 2 shows the flowchart of the above implementation. The source term $b'$ in the pressure correction equation is the continuity imbalance arising from the incorrect velocity field $u^*$, $v^*$. The details of pressure correction equation and the definition of $d$ are provided in the book by Versteeg and Malalasekera [21]. The above procedure can be simply extended to 3-D flows.

As mentioned earlier, the volume fraction ($\phi$) is defined separately for $u$, $v$, and $p$-cells. Thus, in the evaluation of Eqs. (24) and (26) and defining mass and inertia of the particles, one should use the proper volume fraction for $u$, $v$, or $p$-cells to satisfy Eq. (27) and the similar equation for torque applied to the particles.

## 4. Collision strategy

Several studies on the rebound of colliding particles have been published in recent years (e.g. [22,23] and [19]). Davis et al. [24] employed an elastohydrodynamic model for collision between particles suspended in a liquid. They showed that the pertinent parameter for collision in the fluid is not the Reynolds number, $Re$, but the Stokes number $St = \frac{1}{9}\frac{\rho_{\mathrm{p}}}{\rho_{\mathrm{f}}}Re$ where $\rho_{\mathrm{p}}$ and $\rho_{\mathrm{f}}$ are the particle and fluid densities, respectively and $Re = \frac{\rho_{\mathrm{f}}U_iD}{\rho_{\mathrm{f}}}$; $U_i$ is the impact velocity and $D$ is the particle diameter. No rebound occurs for Stokes number lower than about 10 due to the fact that the elastic energy stored by the particle deformation is dissipated in the fluid. For impact Stokes numbers larger than about 500, the coefficient of restitution asymptotes to that for a dry collision.

In this section, we consider the collision between particles when the Stokes number is smaller than 10 or no rebound occurs. For Stokes number larger 10, rebound occurs and the collision strategy detailed by Ardekani and Rangel [19], which is able to handle general shape objects and larger number of particles, should be used. The collision process in this method starts when the separation between particles is zero for smooth particles or equal to the roughness height ($h_{\min}$) for particles with a rough surface. We assume that rough surfaces have small bumps with dilute surface coverage and that there negligible effect on the viscous force until the gap between the smooth portions of surfaces become equal to the size of largest roughness element. For example, considering two particles of the same diameter and different surface roughness colliding onto a wall, they have the same behavior until the particle with larger roughness hits the wall. The difference between these two cases is that the collision starts earlier for the particle with the larger surface roughness. For a frictionless collision, the tangential force is zero while the same normal force applies to each particle in opposite directions as shown in Fig. 3. In the present method, upon collision of particles, a contact force is applied to each particle and the relative velocity of the particles along their line of center vanishes. Using the preceding concepts during the collision process, we write

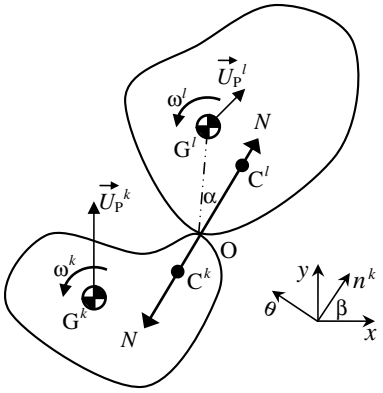


**Fig. 3.** Schematic of problem and coordinate systems.

$$N = N^* + \delta N, \quad \delta N = C'(\mathbf{U}_C^l - \mathbf{U}_C^k)\cdot \mathbf{n}^k \tag{28}$$

$$F_{xi,J}^k = F_{xi,J}^k + \delta N \cos(\beta) A_{i,J}\rho_P^k \phi_{u_{i,j}}^k / M_{P_u^k} \tag{29}$$

$$F_{yI,j}^k = F_{yI,j}^k + \delta N \sin(\beta) A_{I,j}\rho_P^k \phi_{v_{I,j}}^k / M_{P_v^k} \tag{30}$$

$$M_{P_u^k} = \sum A_{i,J}\rho_P^k \phi_{u_{i,J}}^k, \quad M_{P_v^k} = \sum A_{I,j}\rho_P^k \phi_{v_{I,j}}^k \tag{31}$$

where $\mathbf{U}_C$ represents velocity of point $C$ which is the center of curvature at contact point, $k$ and $l$ are the particle indices. For a system of two particles, $k = 1, 2$ and $l = 1, 2$. These calculations guarantee that

$$\int_{P^k} \mathbf{F}^k \, d\mathbf{x} = N\mathbf{n}^k \tag{32}$$

$C'$ is a dimensional constant defined as $C' = \alpha'(M_{pl} + M_{pk})U_s/D$ where $\alpha'$ is a dimensionless factor whose values are also provided in Section 5, and $D$ is the problem length scale which is the particle diameter.

For non-spherical (or non-cylindrical in 2-D) particles the force due to collision may lead to a torque around center of mass of each particle. In this situation, the uniform distributed force is modified in order to create a net torque around the center of mass of each particle without changing the net force applied to that particle. Thus, we have

$$\delta T^k = \overrightarrow{G^k O} \times (\delta N \mathbf{n}^k) \tag{33}$$

$$F_{xi,J}^k = F_{xi,J}^k - \delta T^k A_{i,J}\rho_P^k \phi_{u_{i,j}}^k (y_J - y_G^k)/I_{xxp^k} \tag{34}$$

$$I_{xxp^k} = \sum A_{i,J}\rho_P^k \phi_{u_{i,j}}^k (y_J - y_G^k)^2 \tag{35}$$

where $y_G^k$ is the vertical position of the center of mass of particle $k$. This modified force distribution still satisfies Eq. (32). Moreover

$$\int_{P^k} \mathbf{r} \times \mathbf{F}^k \, d\mathbf{x} = T^k \mathbf{k} \tag{36}$$

where $T^k$ is the net torque applied to particle $k$ due to collision and $\mathbf{k}$ is the unit vector along $z$ direction. Eqs. (28)–(36) will be solved for particle $l$ as well. For multi-particle systems, the procedure is the same as explained above but $k$ and $l$ take values to cover all possible collisions between particles.

The contact force is impulsive at the onset of the collision process and decreases smoothly to zero when contact ends. Particles separate from each other when the contact force vanishes and subsequently, a rigidity constraint is satisfied for each particle separately.

In Fig. 2, these equations will be solved at the step denoted ★. The conditions at which collision occurs will be verified at the step denoted ★★. In the present method, we can calculate the contact force between particles and this is used as a criterion to determine the end of the collision process. No other repulsive force is employed. Since the contact force is calculated, this method can be generalized to frictional collisions. For 3-D calculation, $F_z$ will be calculated in the same way as Eqs. (29) and (30).

The time step can be adjusted so that when particles come into contact there is no overlap. If a fixed time step were used, the particles could overlap when they come close to each other. In order to prevent this overlap, the time step should be adjusted in such a way that the particles come into contact within a specified tolerance. An upper limit should set for the time step to assure that particles do not overlap upon collision. $t^{n+1} - t^n < d^n/|U_r^n|$ where $d^n$ is the separation between particles at the $n$th time step and $|U_r^n|$ is the relative velocity of the particles towards each other (along the line of centers). In

general, this limit might not guarantee that the particles do not overlap. However, in the problem of colliding particles, the deceleration of the particles before collision prevents an overlap.

## 5. Results and discussion

### 5.1. Flow past a stationary circular cylinder

As in the first case, the flow past a stationary circular cylinder is modeled. This case is designed to test the solution process without the added complication of the particle motion and collision. Fig. 4 shows the geometry used for this case. The boundary conditions are

- $u = U_{\text{in}}, v = 0$ on the left (inlet flow) boundary.
- $\frac{\partial v}{\partial y} = 0, \frac{\partial u}{\partial y} = 0$ on the top and bottom boundaries.
- $\frac{D\mathbf{u}}{Dt} = 0$ on the right (exit flow) boundary.

For fixed objects we have

$$\mathbf{u}_{\text{P}} = 0 \quad \text{and} \quad \mathbf{u}_{\text{R}} = \mathbf{u}(1-\phi) \tag{37}$$

The drag force can be determined by calculating the summation of $\mathbf{F}$ in the particle domain. Table 1 shows a summary of results for different Reynolds numbers where $C_{\text{D}}$ is the drag coefficient and $L$ represents the ratio of circulation length to the particle diameter. The results compare very favorably with both experimental and previous computational results.

For the data presented in Table 1, the mesh size is $\frac{1}{11}$ of the particle radius. As it is shown in Fig. 4, the domain size is $30 \times 60$ times the particle radius for $Re > 4$. The geometry used for $Re = 1$ and $Re = 4$ is different from the one shown in Fig. 4. Since the upstream flow is affected by the presence of the cylinder as much as the downstream flow, we double the width of the flow domain and the center of the cylinder is moved towards the center of the computational domain.

#### 5.1.1. Unsteady vortex shedding: $Re = 100$

For higher Reynolds number, instability occurs and the classic oscillatory wake behind the cylinder can be easily captured. In Fig. 5, we plot lift, drag, and torque coefficients, $C_{\text{L}}$, $C_{\text{D}}$, $C_{\text{T}}$ versus non-dimensional time $\frac{tU_{\text{in}}}{D}$, respectively, at $Re = 100$ where $D$ is the diameter of particle. The forces which impose zero velocity field in the particle domain are equal to the reaction forces applied on the cylinder to fix it. Therefore, the lift and drag coefficients can be calculated easily just by calculating the summation of $F_y$ and $F_x$ in the particle domain, respectively.

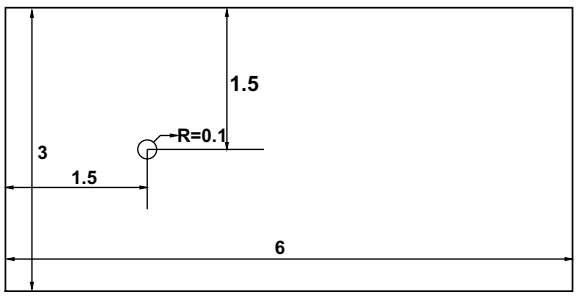


**Fig. 4.** Relative position of cylinder and boundaries.

**Table 1**
Summary of results for $1 < Re < 40$

| | $C_{\text{D}}(L)$ | | | | | |
|---|---|---|---|---|---|---|
| *Re* | 1 | 4 | 10 | 20 | 30 | 40 |
| Takami and Keller [25] | 10.28 | 4.44 | 2.75 (0.25) | 2.00 (0.93) | 1.72 (1.61) | 1.54 (2.32) |
| Dennis and Chang [26] | – | – | 2.85 (0.26) | 2.05 (0.94) | – | 1.52 (2.35) |
| Fornberg [27] | – | – | – | 2.00 (0.91) | – | 1.50 (2.24) |
| Calhoun [28] | – | – | – | 2.19 (0.91) | – | 1.62 (2.18) |
| Present work | 11.11 | 4.65 | 2.88 (0.24) | 2.08 (0.90) | 1.75 (1.57) | 1.55 (2.23) |

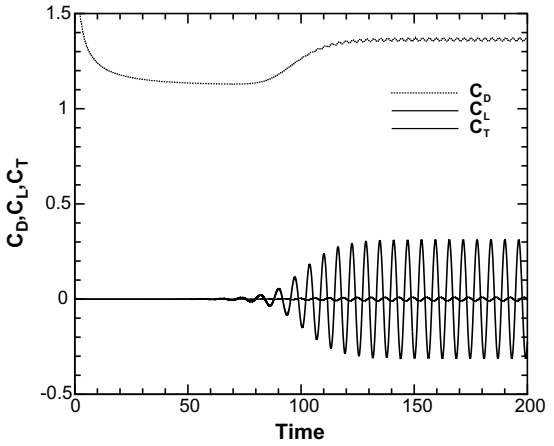


**Fig. 5.** Time dependent lift, drag, and torque coefficients at $Re = 100$.

$$C_D = \frac{\Sigma F_x}{1/2\rho_f U_{in}^2 D}$$
$$C_L = \frac{\Sigma F_y}{1/2\rho_f U_{in}^2 D}$$
$$C_T = \frac{-\Sigma F_x(y - y_G) + \Sigma F_y(x - x_G)}{1/4\rho_f U_{in}^2 D^2} \quad (38)$$

The summary of results is shown in Table 2. Generally, our results are well within the range of results reported by other researchers.

The validation of the fluid-particle solver for moving objects and collisions between a spherical particle and a wall and two cylindrical objects is discussed by Ardekani and Rangel [19]. Here, we present results for collision of general shape objects and cases with more than two particles.

### 5.2. Sedimentation of three circular particles in a two dimensional channel

In this section, we present the sedimentation of three circular particles in a Newtonian fluid inside a vertical channel. All dimensional quantities in this paper are in the CGS system unless otherwise stated. The fluid density is $\rho_f = 1$, the acceleration of gravity is $g = 981$, the viscosity is $\mu = 0.01$, the particle diameters are 0.25 and the solid-to-fluid density ratio is 1.5. Particles are released from rest in a channel with a width of 2.5 and a height of 6. The particles are initially at the center of the channel at $y_1 = 1.5$, $y_2 = 2$, and $y_3 = 2.45$. The Reynolds number based on the maximum velocity of the particles is 650. The normal derivative of velocity is zero at the downstream boundary. In order to reduce computational cost by using a smaller domain, modelling is performed in a frame of reference moving with a fixed velocity close to the average velocity of particles. The mesh sizes is 0.012 and time steps is 0.00025.

The lubrication force acting on two cylinders is linearly proportional to $h^{-\frac{3}{2}}$ and hence, the cylinders do not touch in finite time. However, in a numerical simulation, an infinitesimal grid spacing is necessary to prevent contact, which is not computationally affordable. One could use lubrication theory when the cylinders are sufficiently close to obtain an approximate solution. In the simulations presented here, the cylinders are not smooth but have a roughness of $h_{min} = 0.5\%D$.

Fig. 6 shows the characteristic drafting, kissing, and tumbling behavior of three sedimenting particles. The leading particle creates a wake of low pressure. The middle and trailing particles are caught in its wake. The middle one experiences the lowest drag hence falls faster than the other two. The increased speed of the middle particle produces a collision (kissing con-

**Table 2**
Summary of results for $Re = 100$

| | $C_D$ | $C_L$ | $St$ |
|---|---|---|---|
| Braza et al. [29] | $1.36 \pm 0.015$ | ±0.25 | – |
| Liu et al. [30] | $1.35 \pm 0.012$ | ±0.339 | 0.164 |
| Calhoun [28] | $1.33 \pm 0.014$ | ±0.298 | 0.175 |
| Russell and Wang [31] | $1.34 \pm 0.007$ | ±0.276 | 0.165 |
| Present work | $1.36 \pm 0.0085$ | ±0.310 | 0.163 |

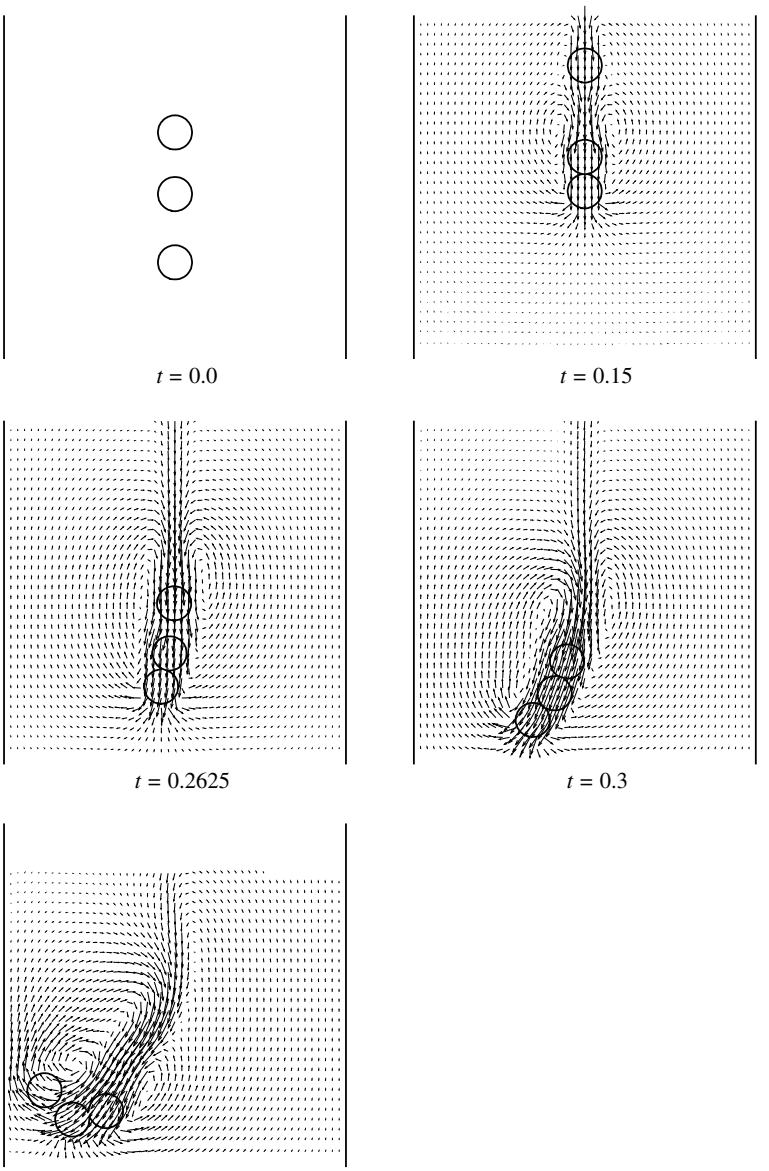


tact) with the leading particle. During kissing contact, the two particles form a long body with the line of centers along the
am. This state is unstable in a Newtonian fluid and as a result the particles tumble under the influence of a couple which
lem into a broadside stable state. Before the separation of the leading and middle particles, a second collision be-
he trailing and middle particles occurs. At this point, the system forms a long body and on average, the line of centers
e across the stream. As they rotate, the normal force between the leading and middle particles decreases to zero and
separate. Finally, the middle and trailing particles separate.

ig. 7 shows the $u$ and $v$ velocity of the particles. The first collision occurs at $t = 0.143$ and the second collision occurs at
= 0.285.

Fig. 8 shows the effect of mesh size and time step on the motion of the particles. Fig. 9 shows the error in the maximum velocity of the middle particle before collision as a function of mesh size and time step. The slope of the error plot reveals that the current implementation of the scheme is second-order accurate with respect to the grid size and time step.

Different values of $\alpha$ and $\alpha'$ were chosen to investigate how these parameters affect the number of iterations needed for convergence each time step. The different values of $\alpha$ and $\alpha'$ do not affect the converged solution. The value chosen, num-

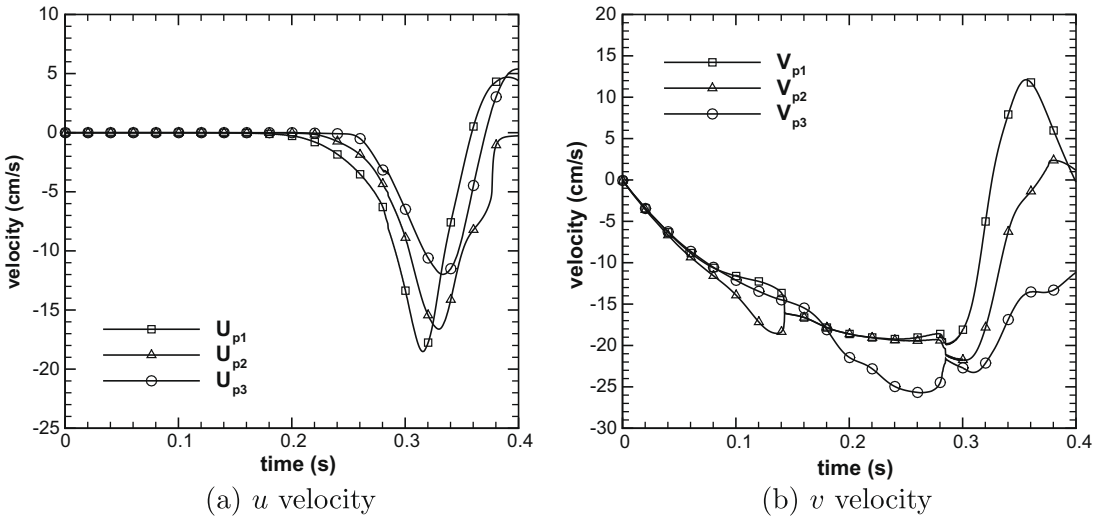


**Fig. 7.** Sedimentation of three circular particles. The mesh size is 0.012 and the time step is 0.00025.

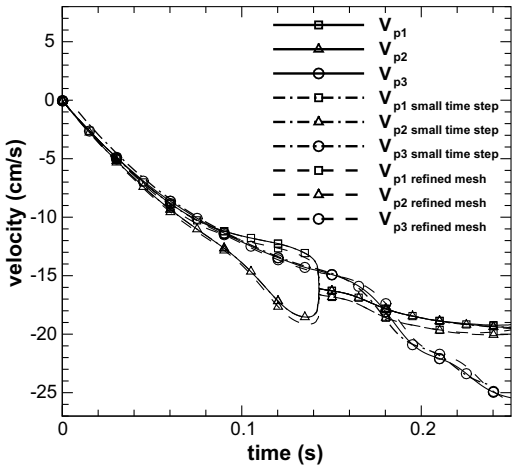


**Fig. 8.** Sedimentation of three circular particles vs component of particle velocity for three cases are compared. The first case has a mesh size of 0.012 and a time step of 0.00025. In the second case, the mesh size is 0.012 and the time step is 0.000125. In the third case, the mesh size is 0.008 and the time step is 0.00025.

ber of iterations needed for convergence at each time step, and CPU time using a PC (Pentium 4, CPU 3.00 GHz) for selected time before and after collision are shown in Table 3.

We should mention that there is no separate iteration for collision. New residuals are defined for rigidity and collision and the outer iteration converges when all the residuals are small enough. This scheme can be expensive for dense particulate flows if particles have small roughness. As such this approach may not be as effective in the really challenging multi-particle scenarios of smooth particles. No other collision models can handle collision of smooth particles unless those which switch to a lubrication model when the particles are close to each other. For particulate flow with large surface roughness, the number of iterations needed to calculate the force acting on a particle is of the same order as those needed to solve momentum and continuity equations. For a case with $\alpha = 10$, $\alpha' = 1$, when no particles are in contact, 79 iterations are in average needed for convergence at each time step. When two and three particles are in contact 91 and 140 iterations are needed, respectively.

The residual for the sedimentation of two circular particle is shown in Fig. 10. The variables $u$, $v$, and $p$ correspond to the normalized residual of $x$ momentum, $y$ momentum, and continuity equation over the entire domain, respectively. The variables $u_{R1}$, $v_{R1}$, $u_{R2}$, and $v_{R2}$ correspond to the normalized residuals of the rigidified velocity over the particle domain along the $x$ and $y$ directions for particles 1 and 2, respectively. $U_c$ is the normalized residual for the conservation of linear momentum during the collision process along the particles line of center. $U_c$ is zero before collision.

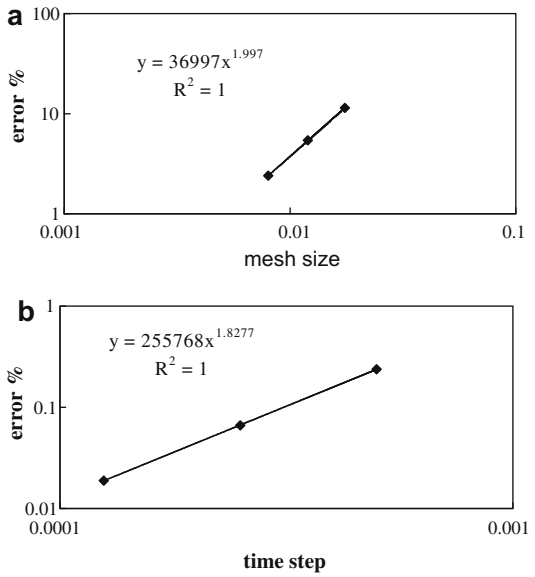


**Fig. 9.** The error in the maximum velocity of the middle particle before collision as a function of mesh size and time step.

**Table 3**
Number of iterations for different values of $\alpha$ and $\alpha'$

| $\alpha$ | $\alpha'$ | Time (s) | Number of iterations | CPU time (s) |
|---|---|---|---|---|
| *Before collision* | | | | |
| 5 | 1 | 0.12550–0.12575 | 182 | 82 |
| 10 | 1 | 0.12550–0.12575 | 92 | 62 |
| 5 | 2 | 0.12550–0.12575 | 176 | 111 |
| *After collision* | | | | |
| 5 | 1 | 0.16175–0.16200 | 181 | 82 |
| 10 | 1 | 0.16175–0.16200 | 91 | 50 |
| 5 | 2 | 0.16175–0.16200 | 181 | 104 |

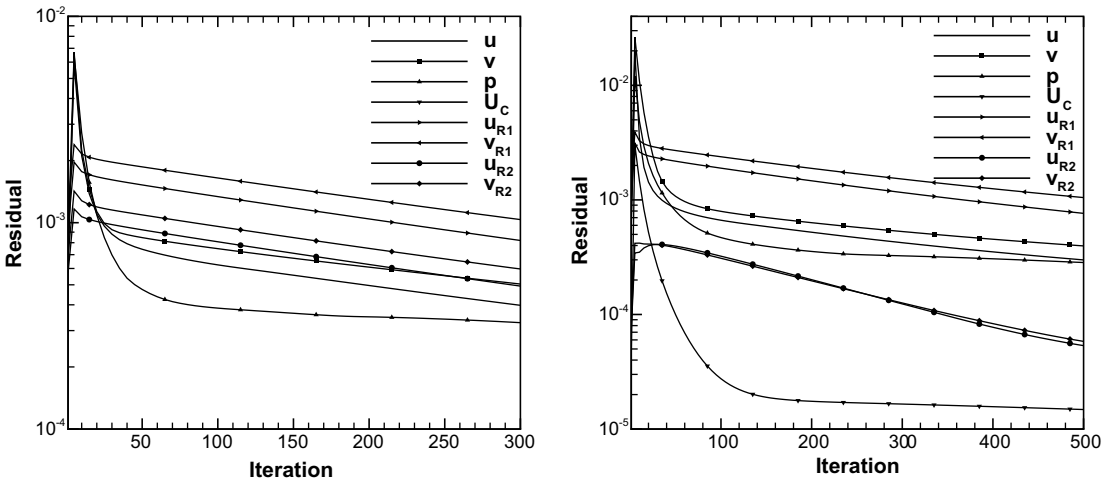


(a) before collision (b) after collision

**Fig. 10.** Residual for the sedimentation of two circular particles. The mesh size is 0.012 and the time step is 0.00025.

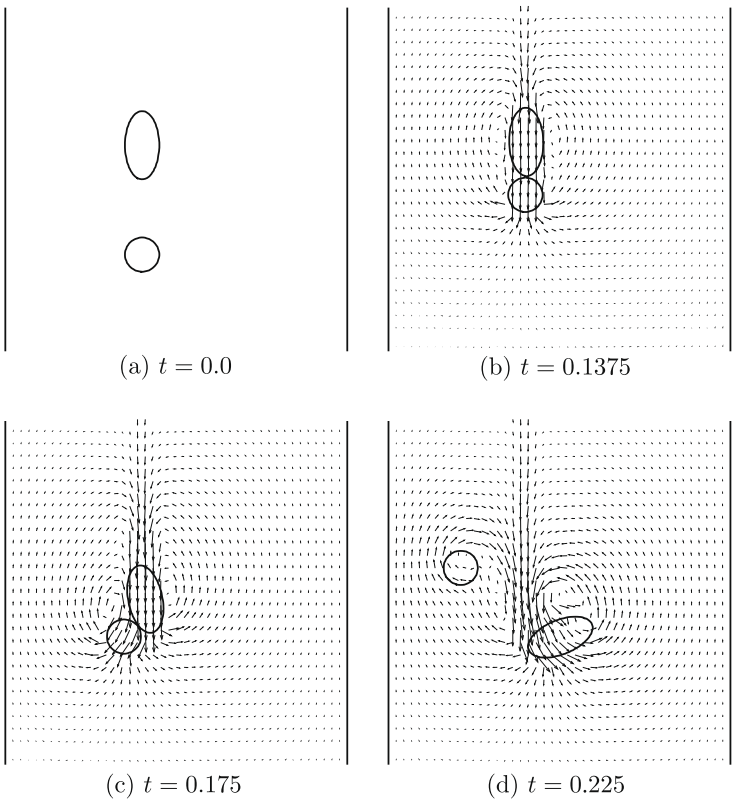


**Fig. 11.** Sedimentation of an ellipse and a circular particles. The mesh size is 0.013 and the time step is 0.00025.

### 5.3. Sedimentation of elliptical and circular particles in a two dimensional channel

In order to show the capability of the algorithm for general shape objects, the sedimentation of elliptical and circular particles is investigated. Other conditions are similar to those in the previous case. The particles are initially $\Delta x = 0.25$ off the center of the channel at $y_1 = 1.5$ and $y_2 = 2.3$. The diameter of the circular particle is 0.25 and the diameters of the elliptical particle are 0.25 and 0.5. A moving computational domain is used and the boundary conditions are the same as in the previous case. The mesh sizes is 0.013 and the time step is 0.00025.

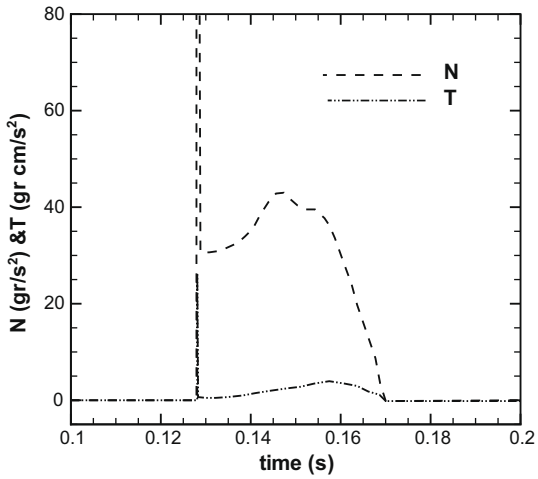


**Fig. 12.** Normal force and the torque applied to an ellipse. The mesh size is 0.013 and the time step is 0.00025.

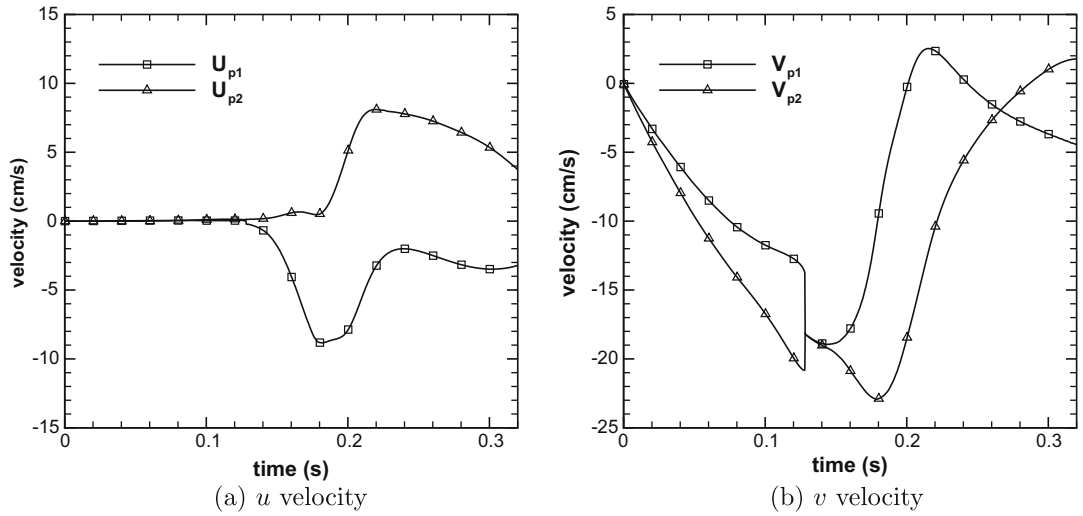


**Fig. 13.** Sedimentation of an ellipse and a circular particles. The mesh size is 0.013 and the time step is 0.00025.

The ellipse is placed in the wake of the leading circular particle and experiences a lower drag force. The initial long side along-the-flow position is changed to a broad side position during the fall of the ellipse. As the particles sediment, collision occurs and the ellipse slips over the sphere (see Fig. 11). As they tumble, the contact force decreases and they separate. The normal force and the torque acting on the ellipse are shown in Fig. 12. Fig. 13 shows the velocity components. The collision occurs at $t = 0.12825$.

## 6. Conclusions

A finite-volume distributed-Lagrange-multiplier algorithm is developed to solve particulate flows with collisions. A collision strategy is introduced for multi-particle system and general shape objects. In this method, the contact force between particles is calculated and the method can be generalized for collisions including friction.

## Acknowledgement

We are grateful to Professor N.A. Patankar for the motivation to this work.

## References

[1] R.H. Davis, Elastohydrodynamic collisions of particles, PCH PhysicoChem. Hydrodyn. 9 (1987) 41–52.
[2] R.H. Davis, Effect of surface roughness on a sphere sedimenting through a dilute suspension of neutrally buoyant spheres, Phys. Fluids 4 (1992) 2607–2619.
[3] S. Zeng, E. Kerns, R.H. Davis, The nature of particle contact in sedimentation, Phys. Fluids 8 (1996) 1389.
[4] M. Ekiel-Jezewska, F. Feuillebois, N. Lecoq, K. Masmoudi, R. Anthore, F. Bostel, E. Wajnryb, Hydrodynamic interactions between two spheres at contact, Phys. Rev. E 59 (1999) 3182.
[5] M. Ekiel-Jezewska, N. Lecoq, R. Anthore, F. Bostel, F. Feuillebois, Rotation due to hydrodynamic interactions between two spheres in contact, Phys. Rev. E 66 (2002) 051504-1–051504-14.
[6] J. Zhang, L. Fan, C. Zhu, R. Pfeffer, D. Qi, Dynamic behavior of collision of elastic spheres in viscous fluids, Powder Tech. 106 (1999) 98–109.
[7] J. Lin, Y. Wang, J. Olsen, Sedimentation of rigid cylindrical particles with mechanical contacts, Chin. Phys. Lett. 22 (2004) 628–631.
[8] J.F. Brady, G. Bossis, Stokesian dynamics, Annu. Rev. Fluid Mech. 20 (1988) 111–157.
[9] A.M. Ardekani, R.H. Rangel, Unsteady motion of two solid spheres in Stokes flow, Phys. Fluids 18 (2006) 103306-1–103306-14.
[10] R. Glowinski, T.W. Pan, J. Periaux, Distributed Lagrange multiplier method for incompressible viscous flow around moving rigid bodies, Comput. Methods Appl. Mech. Eng. 151 (1998) 181–194.
[11] R. Glowinski, T.W. Pan, T.I. Hesla, D.D. Joseph, A distributed Lagrange multiplier fictitious domain method for particulate flows, Int. J. Multiphase Flow 25 (1999) 755–794.
[12] N.A. Patankar, P. Singh, D.D. Joseph, R. Glowinski, T.W. Pan, A new formulation of the distributed Lagrange multiplier/fictitious domain method for particulate flows, Int. J. Multiphase Flow 26 (2000) 1509–1524.
[13] N.A. Patankar, A formulation for fast computations of rigid particulate flows, Center Turbulence Res. Annu. Res. Briefs (2001) 185–196.
[14] N. Sharma, Y. Chen, N.A. Patankar, A distributed Lagrange multiplier based computational method for the simulation of particulate-stokes flow, Comput. Methods Appl. Mech. Eng. 194 (2005) 4716–4730.
[15] S.V. Patankar, Numerical Heat Transfer and Fluid Flow, McGraw-Hill, New York, 1980.
[16] P. Singh, D.D. Joseph, T.I. Hesla, R. Glowinski, T.W. Pan, Direct numerical simulation of viscoelastic particulate flows, J. Non-Newton. Fluid Mech. 91 (2000) 165–188.
[17] P. Singh, T.I. Hesla, D.D. Joseph, Distributed Lagrange multiplier method for particulate flows with collisions, Int. J. Multiphase Flow 29 (2003) 495–509.
[18] H.H. Hu, N. Patankar, M.Y. Zhu, Direct numerical simulations of fluid–solid systems using the arbitrary Lagrangian–Eulerian technique, J. Comput. Phys. 169 (2001) 427–462.

[19] A.M. Ardekani, R.H. Rangel, Numerical investigation of particle–particle and particle-wall collisions in a viscous fluid, J. Fluid Mech. 596 (2008) 437–466.
[20] N. Sharma, N.A. Patankar, A fast computation technique for direct numerical simulation of rigid particulate flows, J. Comput. Phys. 205 (2005) 439–457.
[21] H. Versteeg, W. Malalasekra, An Introduction to Computational Fluid Dynamics, Longman Scientific and Technical, New York, 1995.
[22] G. Joseph, R. Zenit, M. Hunt, A. Rosenwinkel, Particle-wall collisions in a viscous fluid, J. Fluid Mech. 433 (2001) 329–346.
[23] P. Gondret, E. Hallouin, M. Lance, L. Petit, Experiments on the motion of a solid sphere toward a wall: from viscous dissipation to elastohydrodynamic bouncing, Phys. Fluids 11 (1999) 2803–2805.
[24] R.H. Davis, J.M. Serayssol, E.J. Hinch, The elastohydrodynamic collision of two spheres, J. Fluid Mech. 163 (1986) 479.
[25] H. Takami, H.B. Keller, Steady two-dimensional viscous flow of an incompressible fluid past a circular cylinder, Phys. Fluids 12 (1969) II51–II56.
[26] S.C.R. Dennis, G.Z. Chang, Numerical solutions for steady flow past a circular cylinder at Reynolds number up to 100, J. Fluid Mech. 42 (1970) 471.
[27] B. Fornberg, A numerical study of steady viscous flow past a circular cylinder, J. Fluid Mech. 98 (1980) 819–855.
[28] D. Calhoun, A Cartesian grid method for solving the two-dimensional streamfunction-vorticity equations in irregular regions, J. Comput. Phys. 176 (2002) 231–275.
[29] M. Braza, P. Chassaing, H.H. Minh, Numerical study and physical analysis of pressure and velocity fields in the near wake of a circular cylinder, J. Fluid Mech. 165 (1986) 79–130.
[30] C. Liu, X. Zheng, C.H. Sung, Preconditioned multigrid methods for unsteady incompressible flows, J. Comput. Phys. 139 (1998) 35–57.
[31] D. Russell, Z.J. Wang, A Cartesian grid method for modeling multiple moving objects in 2D incompressible viscous flow, J. Comput. Phys. 191 (2003) 177–205.